Harmonics Effects on Microwave Power Measurement Using Diode Sensors

Karel Dražil, Jan Grajciar, Tomáš Pavlíček, Murat Celep, and Martin Hudlička, *Senior Member, IEEE*

***Abstract*— This paper investigates the influence of second and third harmonic components in the signal on a measured RF power level when diode power sensors are employed. The impact of the harmonic components is first demonstrated through the modeling of diode detectors for the worst case scenario. We proposed an approximate general formula for calculating measurement errors due to the higher harmonic components. A method for the measurement of the sensitivity of diode power sensors on the higher harmonic components is also described. Finally, we validated our model with experimental data for several power sensors.**

***Index Terms*— Diode detector, harmonic effect, microwave measurements, microwave power, power sensor.**

I. Introduction

At RF and microwave frequencies, power has been adopted as the primary amplitude measurement quantity for the signal. The metrological traceability of microwave power to the international system of units (SI) is provided through a microcalorimeter setup typically around 0 dBm nominal power [1] with thermistor sensors used as transfer standards. Thermistor sensors are suitable for the most accurate power measurements in metrological laboratories but they are not very suitable for most practical applications. One of the main limitations of thermistors includes their low dynamic range (maximum 30 dB). For most applications, diode-type power sensors (DTPSs) with significantly higher dynamic range (50 dB to 90 dB) are widely used, allowing power levels in the range from −70 dBm to +20 dBm to be measured. There are currently various types of DTPSs with different internal architecture, which are optimized for various applications.

Diode sensors use high-frequency semiconductor diodes to detect the RF voltage developed across a terminating load resistor. At levels below −20 dBm (22 mV rms input voltage in a 50 Ω system), typical RF diode detectors produce a dc voltage output that is nearly proportional to the square of the applied RF voltage. This is referred to as the square-law or true-rms region. Above 0 dBm, a linear detection (i.e., peak detection) region exists where the output voltage is almost proportional to the input voltage. The transition region of the detectors ranges from approximately −20 dBm to 0 dBm of input power. When operating in the square-law region, detectors tend to measure the true rms power. If a nonsinusoidal signal is to be measured, higher harmonics are weighted according to their power and the error due to harmonics is negligible. However, with an increasing power level, the diode detector changes from rms weighting to peak weighting of the input voltage and the error due to harmonics can significantly increase with dependence on the mutual phase between the fundamental and higher harmonic signal. Graphic presentation of a typical behavior for the R&S DTPS with respect to the second and third harmonics can be found in [2].

Historically, older types of power sensors were designed only for the operation in the square-law regime with a dynamic range approximately 50 dB (e.g., the HP 8484A and Agilent 8481D sensors). With the progress of electronics, it was feasible to construct power sensors featuring detector-shaping compensation [for the continuous-wave (CW) signal] to extend the dynamic range above the square-law region up to 90 dB (e.g., the R&S NRV-Zx, Agilent ECP-26A, or Anritsu MA244xD sensors). There are also latter multipath diode sensors that integrate multiple diode detectors and attenuating power splitters into a single unit. These sensors operate usually with two or three pairs of detectors and select the output of whichever pair is operating in its square-law region. Examples of such architecture include the R&S NRP-Zxx sensors, Keysight U2040 X series, or Anritsu MA2480D series sensors, respectively.

Although some types of DTPS are, under certain conditions, highly susceptible to errors due to harmonics, data supplied by manufacturers are often very limited. To the best of authors' knowledge, detailed information is only available for R&S power sensors where the software [3] is available, which allows to evaluate the measurement uncertainty contributions due to the second and third harmonics. The lack of available information concerning this problem was the main motivation for our work. A method was proposed for the characterization of the influence of higher harmonics on the power meter reading, which gives error bounds provided the input signal harmonic content is known. In [4], the method for power sensor characterization was briefly described and some results were presented. In this paper, a detailed description is given and additional results for other power sensors are demonstrated.

Manuscript received July 10, 2018; revised January 16, 2019; accepted February 25, 2019. Date of current version May 10, 2019. This work was supported by the Project 15RPT01 RFMicrowave through the European Metrology Programme for Innovation and Research (EMPIR) by the Participating States and the European Union's Horizon 2020 Research and Innovation Programme. The Associate Editor coordinating the review process was Djamel Allal. *(Corresponding author: Karel Dražil.)*

K. Dražil, J. Grajciar, T. Pavlíček, and M. Hudlička are with the Czech Metrology Institute, 638 00 Brno, Czech Republic (e-mail: kdrazil@cmi.cz).

M. Celep is with the TUBITAK Ulusal Metroloji Enstitüsü (UME), 41470 Gebze, Turkey.

Color versions of one or more of the figures in this paper are available online at http://ieeexplore.ieee.org.

Digital Object Identifier 10.1109/TIM.2019.2905885

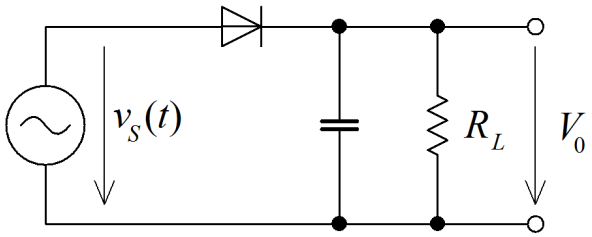

Fig. 1. Simplified equivalent circuit of a single-diode detector.

Only worst case errors were investigated in the frame of our work. The analysis of uncertainty propagation through the measurement model according to guide [5] is out of the scope of this paper.

This paper is organized as follows. In Section II, the worst case errors due to second and third harmonic components are modeled. In Section III, an approximate formula is presented to model the sensor characteristics (in terms of worst case errors) based on empirical data. Section IV discusses the setup for the measurement of the errors caused by higher harmonics. Section V presents measured results for various widely adopted power sensors. In Section VI, potential causes of errors of performed measurements are discussed, and finally, Section VII summarizes this paper.

II. Modeling of Errors Due to Harmonics in Diode Detectors

Modern diode power sensors make use of low-barrier Schottky (LBS), planar-doped barrier (PDB) diodes, or modified barrier integrated diodes (MBID). The ideal I–V characteristic of a detecting diode is given by

$$i_{\mathrm{d}} = I_{\mathrm{S}}(e^{\alpha v_d} - 1) \tag{1}$$

where $\alpha = q/nkT$ and I_{s} is the saturation current, q is the electron charge, k is Boltzmann's constant, T is the absolute temperature, and n is the ideality factor. For a typical detector, $I_{\mathrm{s}} \approx 10\ \mu$A, $n \approx 1.1$ [6]. Equation (1) is often written as the power series

$$i_d = I_{\mathrm{S}}\left(\alpha v_d + \frac{(\alpha v_d)^2}{2!} + \frac{(\alpha v_d)^3}{3!} + \ldots\right). \tag{2}$$

For the purposes of this paper, the detectors are modeled without frequency-dependent elements. A simplified circuit used for modeling is shown in Fig. 1.

The signal with higher harmonics used for investigation is defined as

$$v_S(t) = V_m(\sin(\omega t) + r\sin(m\omega t - \varphi_m)) \tag{3}$$

where V_m is the amplitude of the signal at the fundamental frequency, m is the order of the higher harmonic component, r is the amplitude ratio between the higher and fundamental harmonic components, and φ_m is the phase shift of the mth harmonic component.

The capacitor shown in Fig. 1 is regarded as large enough to keep only the dc voltage. The average current through the diode can be solved by integrating over one RF cycle

$$\frac{1}{T}\int_0^T i_d(t)dt = \frac{V_0}{R_L} \tag{4}$$

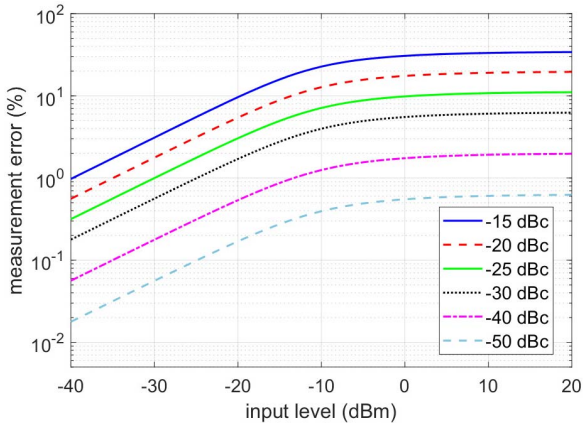

Fig. 2. Modeled worst case errors due to the second harmonic of half-wave detector.

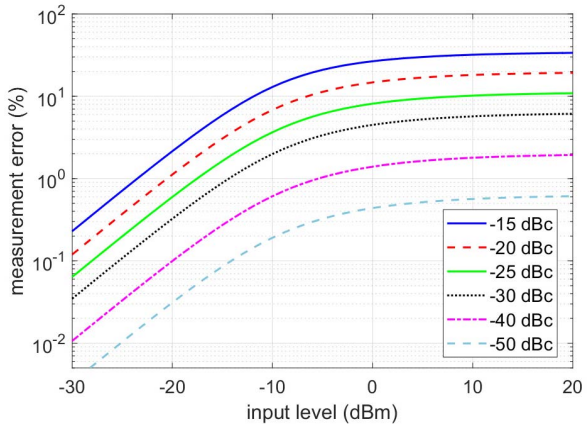

Fig. 3. Modeled worst case errors due to the third harmonic of both detector types.

where V_0 is the dc voltage at the output of the detector. For the detector with an ideal diode shown in Fig. 1

$$i_d(t) = I_S(e^{\alpha(v_S(t)-V_0)} - 1). \tag{5}$$

By solving (3)–(5) numerically, the values for the maximum measurement error of single-diode detectors can be calculated. First, values of detector output voltage V_0 are found iteratively for CW signal and various input voltage levels (presented in dBm at 50 Ω load). Subsequently, the values of total input power are found for the same levels of output voltage V_0, defined harmonic-to-fundamental ratios and various phase shifts. The results obtained are shown in Figs. 2 and 3.

A simplified schematic of a balanced detector with full-wave rectification can be seen in Fig. 4. The detected voltage is now the sum of V_0^+ and V_0^-. As shown in [7], such a detector represents a peak-to-peak rather than just a peak detector for large signals and its sensitivity to the second (and any other even) harmonic is reduced when compared to the single-diode detector. Similarly, we modeled the results for the balanced detector, as shown in Fig. 5.

Results obtained for the detectors with diodes modeled as the exponential device according to (5) can be concluded as follows. Resulting measurement errors due to harmonics seem to be independent on the detector loading resistance R_L. For small R_L, unrealistic current peaks have been calculated

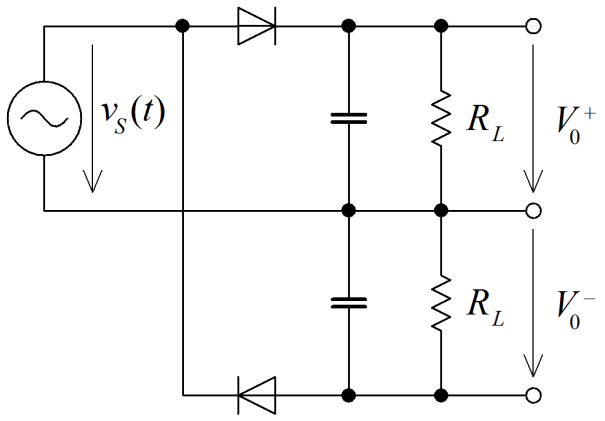

Fig. 4. Simplified equivalent circuit of the full-wave (balanced) detector.

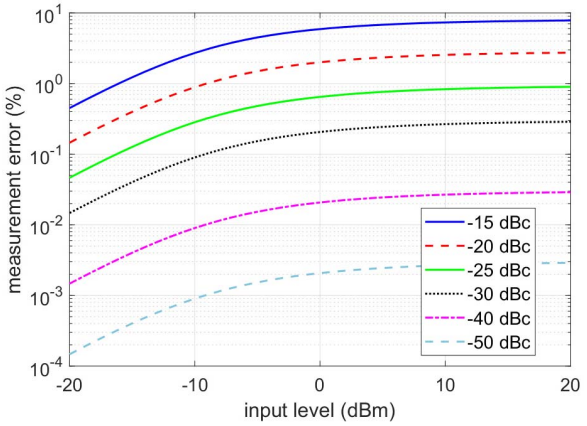

Fig. 5. Modeled worst case errors due to the second harmonic of the full-wave detector.

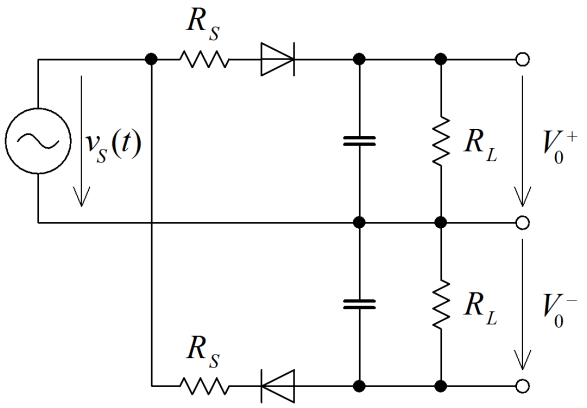

Fig. 6. Equivalent circuit of the balanced detector.

as a consequence of neglecting the resistance in series with the ideal diode model. The shape of the resulting curves in logarithmic scale reveals asymptotic characteristics where the horizontal asymptotes represent the error limits ($\delta \approx 2r$) corresponding to the expected peak detecting behavior of the detectors. Only the horizontal shift of the curves was observed when α was changed. Resultant measurement errors due to harmonics are in very good agreement with those presented in [2].

Fig. 6 shows the model including resistors R_S representing the equivalent Thévenin resistance of the source and ohmic

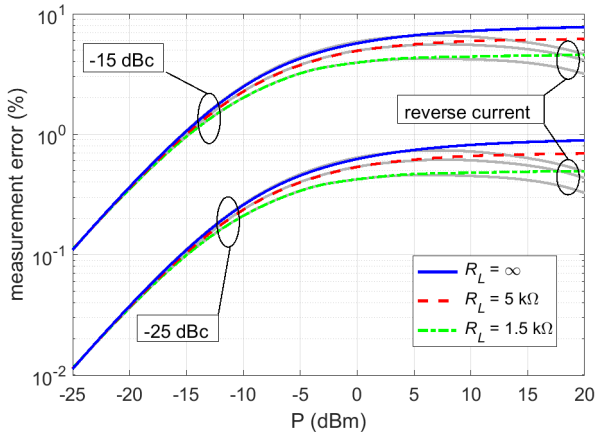

Fig. 7. Modeled worst case errors due to the second harmonic of the full-wave detector.

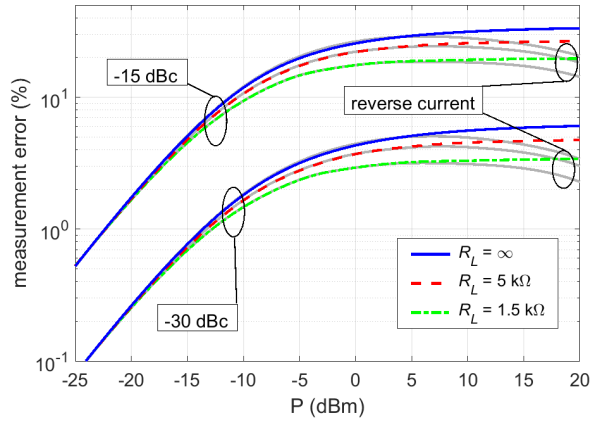

Fig. 8. Modeled worst case errors due to the third harmonic of both detector types.

resistance of the diodes. The numerical results obtained by solving the circuit shown in Fig. 6 can be seen in Figs. 7 and 8 where the effect of the detector load is visible. The effect of the reverse diode current for PDB diodes given in [6] was also modeled.

On the basis of the results, it can be concluded that detectors deviate from the peak-detecting behavior with decreasing loading resistance. This effect can be enforced when the voltage across the diode approaches the breakdown region.

III. Modeling Using the Approximating Formula

The aim of our work was to find a general approximating formula that can help the users to predict the behavior of sensors with respect to harmonics on the basis of only several measurements. Based on the characteristics of the curves, the formula was proposed in the form

$$\delta(\%) = kr^{er}\left[\left(\frac{P_m}{P}\right)^{ep_1 ep_2} + 1\right]^{-\frac{1}{ep_2}} \tag{6}$$

where δ is the maximum measurement error in (%), P is the power level in mW, r is the higher harmonic suppression, P_m and k are the constants optimized for the best fit to the measured or modeled values, ep_2 does influence the bending of the curves and is usually optimized only for the best fit to the modeled values (see Table I), and er and ep_1 are

TABLE I
CONSTANTS FOR THE APPROXIMATING FORMULA

Parameter	2. harm.		3. harm	sensors
	full-wave detector	half-wave detector		
er	2	1	1	
ep_1	1	0.5	1	
ep_2	0.77	1.86	0.85	NRV-Zx
	0.99		1.15	ECP-E26A E4413A

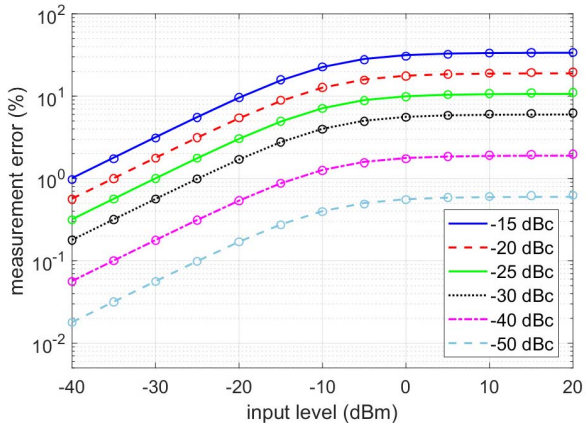

Fig. 9. Worst case errors due to the second harmonic of the half-wave detector, lines = fit by (6), circles = detector model, large R_L.

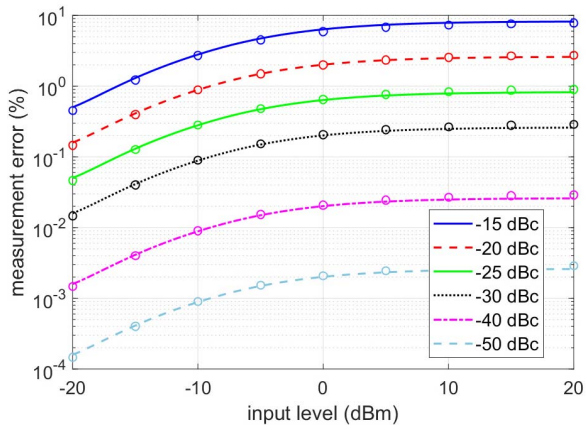

Fig. 10. Worst case errors due to second harmonic full-wave detector, lines = fit by (6), circles = detector modeling, large R_L.

the fixed constants chosen depending on the harmonic order and detector type (see Table I). When the sensor is to be characterized on the basis of measurement, P_m and k are optimized separately for the second and third harmonics.

The results obtained by detector modeling and by (6) are compared in graphs shown in Figs. 9–13. Results for the detectors with large loading resistance (i.e., with peak detecting behavior) can be seen in Figs. 9–11. In Figs. 12 and 13, results for the hypothetical model of the sensor ECP-E26A are compared. This sensor includes 3 dB attenuator at the input, further elements of the model $R_S = 50\ \Omega$, $R_L = 1.4\ \text{k}\Omega$, and the reverse current of the diodes equal to 4 mA at 4 V (see [6]) were supposed. It can be seen that the formula gives acceptable results even for the sensors that do not show the peak detecting

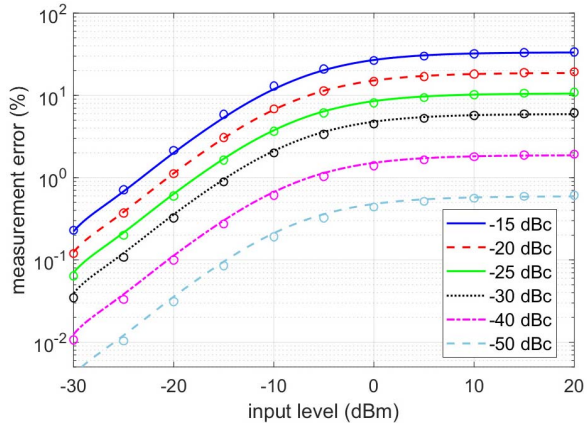

Fig. 11. Worst case errors due to the third harmonic, lines = fit by (6), circles = detector modeling, large R_L.

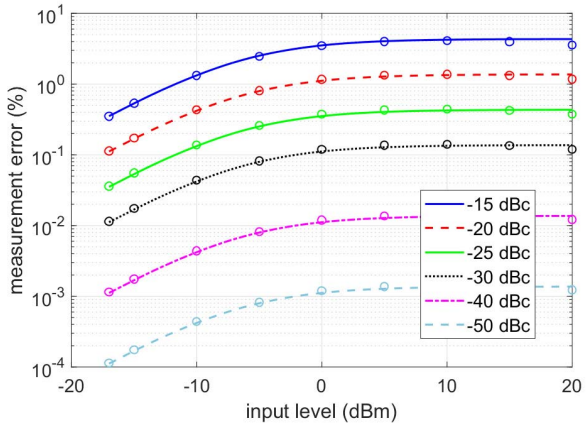

Fig. 12. Worst case errors due to the second harmonic of the full-wave detector, lines = fit by (6), circles = detector model, $R_L = 1.4\ \text{k}\Omega$, reverse diode current taken into account.

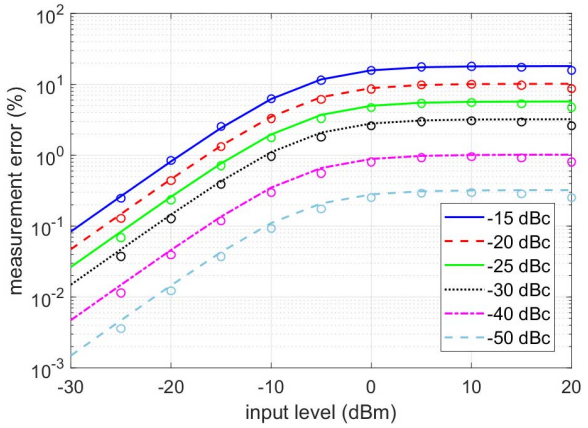

Fig. 13. Worst case errors due to the third harmonic, lines = fit by (6), circles = detector model, $R_L = 1.4\ \text{k}\Omega$, reverse diode current taken into account.

behavior with the potential deviations at levels above 10 dBm taken into account where appropriate.

IV. MEASUREMENT METHOD

The measurement method is based on the fact that the indication of the power meter with DTPS operating above the square-law region is dependent on the phase shift

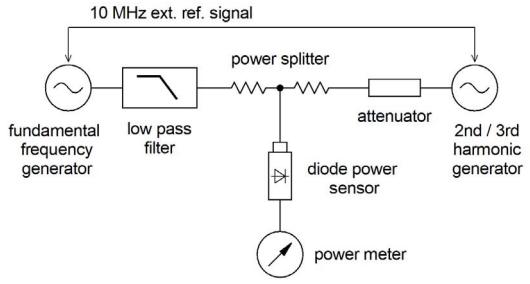

Fig. 14. Setup for the characterization of DTPS with power splitter.

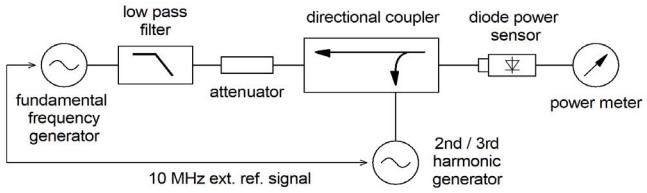

Fig. 15. Setup for the characterization of DTPS with directional coupler.

between the fundamental and higher harmonic components. The measurement setup consists of two RF generators (the fundamental and higher harmonic components) and a coupling device that creates a composite signal. Sufficient isolation of both generators is provided and a set of filters can optionally be used to suppress the unwanted higher order harmonics of the fundamental frequency. The use of phase-locked synthesizers is necessary as the phase shift between the fundamental and higher harmonic components must be adjusted to obtain a maximum/minimum reading of the power meter. The phase shift can be changed between 0° and 360° either directly in the generator (certain types of RF generators have this functionality) or by slightly detuning the frequency of the second generator. The detuning creates a slowly varying change of the power meter reading so that the user can easily monitor the minimum/maximum power reading. Another possibility is to add a suitable variable phase shifter to the input of the reference signal 10 MHz of one of the used synthesizers. The alternative measurement configurations are shown in Figs. 14 and 15. A two-resistor power splitter is used as it yields better isolation between the generators in comparison with the three-resistor power divider. The alternative approach with the directional coupler is suitable, namely, for measurements at higher power levels.

In order to determine the worst case power indication error, it is necessary to find the maximum ($P_{\max}$) and minimum ($P_{\min}$) indicated powers when both the fundamental and higher order harmonic components are present and also when only the fundamental component is present (P_c). Note that the positive and negative errors are not symmetrical, and the larger of them (in magnitude) is to be selected as the result. Especially for the full-wave detector and second harmonic, the positive deviations from the "true" value are significantly more probable (see [7]). The positive and negative errors δ_+ and δ_-, respectively, can be calculated by

$$\delta_+(\%) = \left(\frac{P_{\max}}{P_c(1+r^2)} - 1\right) \cdot 100 \tag{7}$$

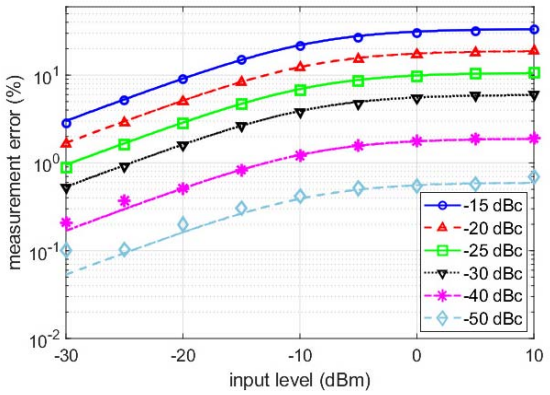

Fig. 16. Modeled and measured worst case errors due to the second harmonic (R&S NRV-Z1 sensor), lines = fit by (6), symbols = measured ($f = 2.5$ GHz).

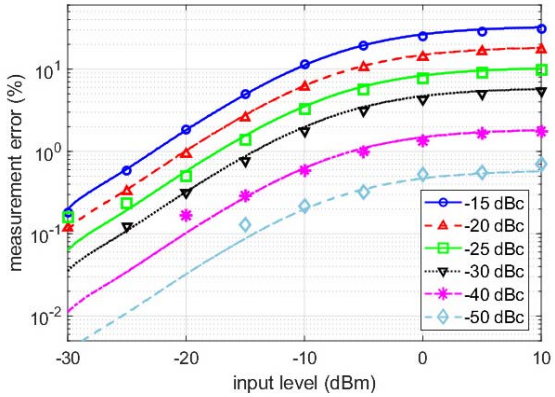

Fig. 17. Modeled and measured worst case errors due to the third harmonic (R&S NRV-Z1 sensor), lines = fit by (6), symbols = measured ($f = 2.5$ GHz).

and

$$\delta_-(\%) = \left(\frac{P_{\min}}{P_c(1+r^2)} - 1\right) \cdot 100 \tag{8}$$

where r is the amplitude ratio between the higher and fundamental harmonic components.

V. Measurement Results

The characterization of the influence of higher harmonic components on the power error was performed for various commercial DTPS from different vendors. Properties of sensors with both half-wave and full-wave detectors, respectively, were evaluated. Figs. 16 and 17 show the results for the R&S NRV-Z1 sensor (half-wave detector). This sensor shows the peak detecting behavior.

Figs. 18 and 19 show the results for the R&S NRV-Z4 sensor (full-wave detector). This sensor also shows the peak detecting behavior.

Figs. 20 and 21 show the results for the HP 8484A sensor (half-wave detector). The characteristics of the sensor cannot be completely fit as the measurement above the square-law region is not supported by the manufacturer.

Figs. 22 and 23 show the results for the sensor HP ECP-E26A (full-wave detector). This sensor does not show the peak-detecting behavior.

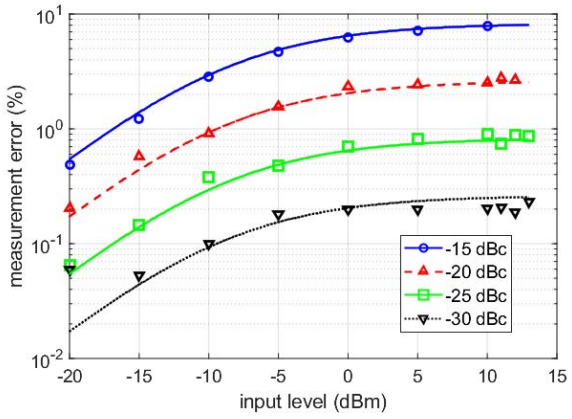

Fig. 18. Modeled and measured worst case errors due to the second harmonic (R&S NRV-Z4 sensor), lines = fit by (6), symbols = measured ($f = 2.5$ GHz).

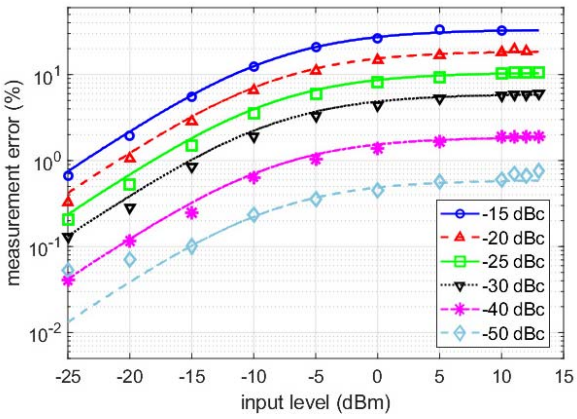

Fig. 19. Modeled and measured worst case errors due to the third harmonic (R&S NRV-Z4 sensor), lines = fit by (6), symbols = measured ($f = 2.5$ GHz).

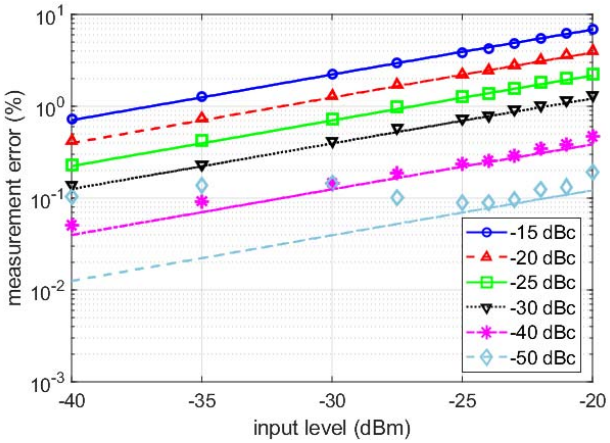

Fig. 20. Modeled and measured worst case errors due to the second harmonic (HP 8484A sensor), lines = fit by (6), symbols = measured ($f = 2.5$ GHz).

Figs. 24 and 25 show the results for the sensor Agilent E4413A (full-wave detector). This sensor does not show the peak-detecting behavior.

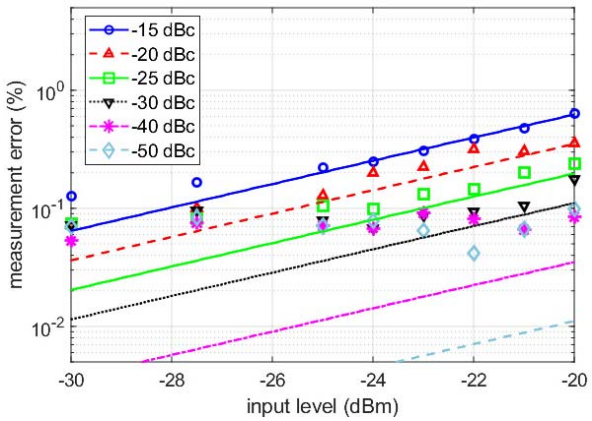

Fig. 21. Modeled and measured worst case errors due to the third harmonic (HP 8484A sensor), lines = fit by (6), symbols = measured ($f = 2.5$ GHz).

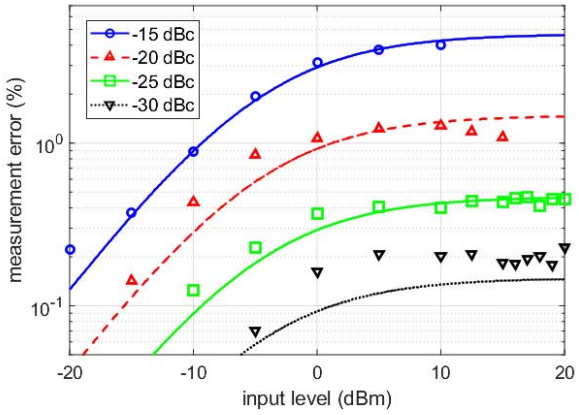

Fig. 22. Modeled and measured worst case errors due to the second harmonic (HP ECP-E26A sensor), lines = fit by (6), symbols = measured ($f = 2.5$ GHz).

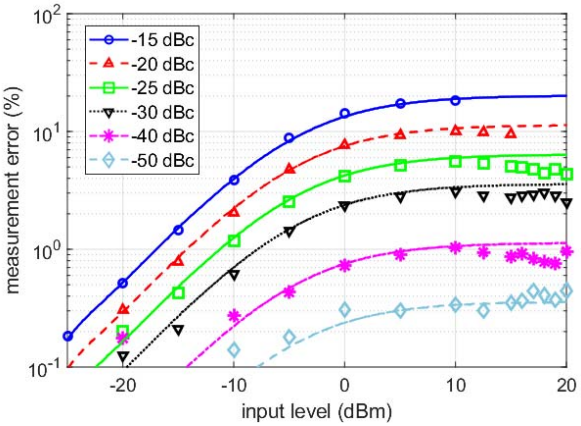

Fig. 23. Modeled and measured worst case errors due to the third harmonic (HP ECP-E26A sensor), lines = fit by (6), symbols = measured ($f = 2.5$ GHz).

VI. Potential Sources of Errors in the Evaluation of the Sensitivity to Harmonics

For practical purposes, the errors caused by the higher harmonics content should only be considered if their size is greater or comparable to other error sources.

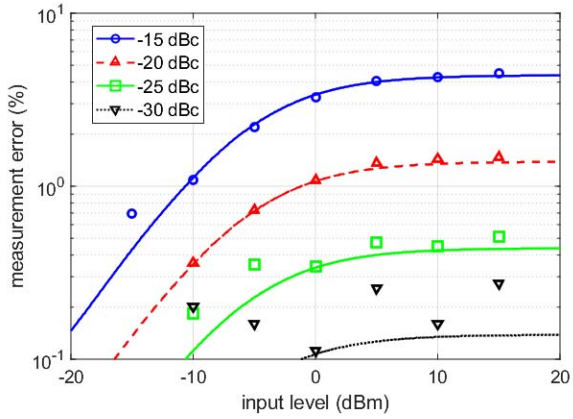

Fig. 24. Modeled and measured worst case errors due to the second harmonic (Agilent E4413A sensor), lines = fit by (6), symbols = measured ($f = 5$ GHz).

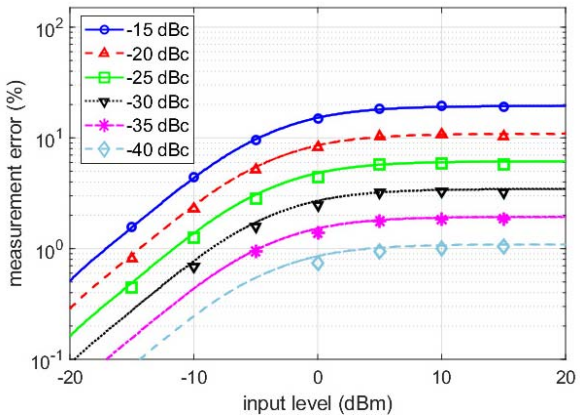

Fig. 25. Modeled and measured worst case errors due to the third harmonic (Agilent E4413A sensor), lines = fit by (6), symbols = measured ($f = 5$ GHz).

When verifying the proposed method, measurements in the region of relatively small expected errors were also performed. Errors in the order of tenths of percent caused by higher harmonics are considered as negligible in practice. As given in Section IV, the errors caused by higher harmonics are evaluated from the changes of the power meter indication, where it is ideally assumed that the changes are only caused by the phase shift change or by switching off the source of the higher harmonic. In the measurements, changes due to noise, zero drift, power meter resolution, and generator output level instability are also evaluated including the influence caused by higher harmonics. These influences tend to be more important for signals with increasing harmonic suppression. In this way, e.g., differences shown in Fig. 21 can be explained.

The measurement setup shown in Figs. 14 and 15 is suitable for frequencies, at which the higher harmonic suppression can be determined using the measured sensor that is capable of working at two or three times of the fundamental frequency. If this condition is not fulfilled, another equipment for the measurement of the level of higher harmonics must be used. It is necessary to keep in mind that the diode sensor connectors are not designed to support the higher harmonic frequencies, where the connector will become overmoded. Consequently, the harmonic response may not be repeatable for higher fundamental frequencies.

Low suppression of higher harmonics of the source of the fundamental frequency may represent an important source of errors. In the case of the measurements presented earlier, signal sources with high suppression of higher harmonics were used together with high-quality filters; thus, this influence can be considered as negligible.

Measurements at higher power levels and for lower harmonic suppressions may be negatively influenced by the mutual interaction of generators due to insufficient isolation and also by reflections between generators and the measured sensor. These errors may be reduced by using a more complex setup with selective leveling possibility for both the fundamental frequency signal and the higher harmonic component.

VII. Conclusion

A method was described for evaluating the influence of higher harmonic components on the measurement error when measuring power using diode power sensors. It was shown for several power sensor types that the errors in the whole dynamic range of the sensors for various harmonic suppressions can be estimated with acceptable accuracy from only several measurements in the transition region above the square-law region with harmonic suppression from approximately −15 dBc to −20 dBc.

It was also shown, by both modeling and measurements, that not all power sensors with detectors operating significantly above the square-law region show the peak detecting behavior.

References

[1] Y. Abdo and M. Celep, "New effective coaxial twin-load microcalorimeter system," in *Proc. Conf. Precis. Electromagn. Meas.*, Jul. 2016, pp. 1–2.

[2] *Voltage and Power Measurements*, document PD 757.0835.23, Rohde & Schwarz, Munich, Germany, 1999.

[3] *Program for Measurement Uncertainty Analysis With Rohde & Schwarz Power Meters*, document AN 1GP43_0E, Rohde & Schwarz Munich, Germany, 2001.

[4] M. Celep, Y. Abdo, K. Dražil, J. Grajciar, M. Hudlicka, and B. Pinter, "Harmonics effects on microwave low-power measurement," in *Proc. Conf. Precis. Electromagn. Meas. (CPEM)*," Jul. 2018, pp. 1–2.

[5] *Evaluation of Measurement Data—Guide to the Expression of Uncertainty in Measurement*, document 100:2008, JGCM, 2008. [Online]. Available: www.bipm.org/en/publications/guides/gum.html

[6] *Fundamentals of RF and Microwave Power Measurements*, document NA 64-1A 5989-6255EN, Agilent, Santa Clara, CA, USA, 1998.

[7] S. Wetenkamp, "Comparison of single diode vs. dual diode detectors for microwave power detection," in *IEEE MTT-S Int. Microw. Symp. Dig.*, Boston, MA, USA, Jun. 1983, pp. 361–363.

Karel Dražil received the Ing. (M.Sc.) degree from the Faculty of Electrical Engineering, Czech Technical University, Prague, Czech Republic, in 1988.

Until 1993, he was with the Research Institute of Radio-Communications, Prague. Since 1993, he has been with the Czech Metrology Institute, Prague. Since 2007, he has been the Head of the Department of Primary Metrology of RF Electrical Quantities, Czech Metrology Institute, Prague. He is involved in national standards of RF power, RF reflection and transmission coefficient, and RF electromagnetic field. His current research interests include precision measurement of scattering parameters and electromagnetic field.

Jan Grajciar received the Ing. (M.Sc.) degree from the Faculty of Electrical Engineering, Czech Technical University, Prague, Czech Republic, in 2015.

He has been a Metrologist and a Researcher with the Czech Metrology Institute, Prague. His current research interests include RF power and vector network analyzer (VNA) measurements.

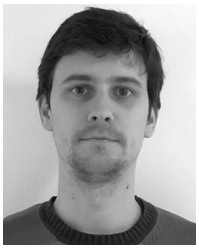

Tomáš Pavlíček received the Ing. (M.Sc.) degree from the Faculty of Electrical Engineering, Czech Technical University, Prague, Czech Republic, in 2013.

He has been a Metrologist and a Junior Researcher with the Czech Metrology Institute, Prague. His current research interests include vector network analyzer (VNA) measurements and modern communication systems.

Murat Celep received the technician degree in electronics from the Tekirdag Vocational School, University of Trakya, Edirne, Turkey, in 1992, and the B.Sc., M.Sc., and Ph.D. degrees from the Department of Electronics and Communication Engineering, Kocaeli University, Izmit, Turkey, in 1999, 2004, and 2013, respectively.

He joined the RF and Microwave Laboratory, TUBITAK Ulusal Metroloji Enstitüsü (UME), Gebze, Turkey, in 1997. He is involved in performing primary and secondary levels of power, S-parameters, impedance, attenuation, and noise measurements at RF and microwave frequencies, installing and characterizing measurement systems, and uncertainty calculations.

Martin Hudlička (S'04–M'08–SM'15) received the Ing. (M.Sc.) and Ph.D. degrees in electrical engineering from the Czech Technical University, Prague, Czech Republic, in 2004 and 2007, respectively.

In 2007, he joined the Department of Primary Metrology of RF Electrical Quantities, Czech Metrology Institute, Prague, where he is a Metrologist and a Researcher. His current research interests include microwave and millimeter-wave measurements and modern communication technologies.